

ANGULAR MOMENTUM TRANSPORT IN ACCRETION DISKS:  
SCALING LAWS IN MRI-DRIVEN TURBULENCEMARTIN E. PESSAH<sup>1,3,4</sup>, CHI-KWAN CHAN<sup>2,4</sup>, AND DIMITRIOS PSALTIS<sup>4,3</sup>*Draft version November 9, 2018*

## ABSTRACT

We present a scaling law that predicts the values of the stresses obtained in numerical simulations of saturated MRI-driven turbulence in non-stratified shearing boxes. It relates the turbulent stresses to the strength of the vertical magnetic field, the sound speed, the vertical size of the box, and the numerical resolution and predicts accurately the results of 35 numerical simulations performed for a wide variety of physical conditions. We use our result to show that the saturated stresses in simulations with zero net magnetic flux depend linearly on the numerical resolution and would become negligible if the resolution were set equal to the natural dissipation scale in astrophysical disks. We conclude that, in order for MRI-driven turbulent angular momentum transport to be able to account for the large value of the effective alpha viscosity inferred observationally, the disk must be threaded by a significant vertical magnetic field and the turbulent magnetic energy must be in near equipartition with the thermal energy. This result has important implications for the spectra of accretion disks and their stability.

*Subject headings:* black hole physics — accretion, accretion disks — MHD — instability — turbulence

## 1. INTRODUCTION

One of the key unsolved problems in accretion disk physics is the precise nature of the mechanism that allows for angular momentum to be transported outwards in the disk. In the standard theory, one copes with this problem by arguing that the stress responsible for angular momentum transport, due to turbulence and magnetic fields, is proportional to the local pressure, i.e.,  $\bar{T}_{r\phi} \equiv q\alpha\bar{P}$ . Here,  $\alpha$  is a dimensionless constant of the order of, but smaller than, unity and  $q \equiv -d\ln\Omega/d\ln r$  characterizes the local shear (Shakura & Sunyaev 1973; Kato, Fukue, & Mineshige 1998; Frank, King, & Raine 2002).

Despite the fact that the standard parametrization leads to a disk model in which the energy generation rate is determined mostly by energy balance and depends weakly on the adopted prescription (Balbus & Papaloizou 1999), almost every aspect of the disk structure depends explicitly on this assumption (Kato, Fukue, & Mineshige 1998; Frank, King, & Raine 2002). Therefore calculating the value of  $\alpha$ , or more generally, testing whether the assumed relationship between stress and pressure is adequate, is of fundamental importance. These questions, however, lie outside the scope of the standard theory, making necessary the identification of a specific physical mechanism for angular momentum transport.

Over the last decade, magnetohydrodynamic (MHD) turbulence driven by the magnetorotational instability (MRI; Balbus & Hawley 1991; 1998) has emerged as the most promising candidate to enable angular momentum transport in astrophysical disks. The development of three-dimensional MHD numerical codes has led to a detailed

study and characterization of angular momentum transport in turbulent magnetized disks. This has motivated numerical estimations of the  $\alpha$  parameter and, more generally, the search for saturation predictors to describe the turbulent state (see, e.g., Hawley et al. 1995, 1996; Brandenburg, Nordlund, Stein, & Torkelsson 1995; Gammie 1998; Pessah, Chan, & Psaltis 2007).

It has long been recognized that the  $\alpha$  parameter is not a constant. It is known to depend, among other things, on the strength and geometry of the magnetic field and, perhaps more uncomfortably, on the size of the simulation domain and the resolution. In spite of this, it has not been possible to disentangle numerical from physical dependencies in a clear way (see, e.g., Hawley et al. 1995, 1996; Brandenburg 1998; Sano, Inutsuka, & Miyama 1998; Sano et al. 2004). Being able to distinguish between these two types of dependencies is vital if we seek to use the results of numerical simulations to build angular momentum transport models, and eventually global disk models, beyond the standard prescription (see, e.g., Kato & Yoshizawa 1995; Ogilvie 2003; Pessah, Chan, & Psaltis 2006b, 2007).

The search for a mechanism for the saturation of the MRI-driven turbulence has been a long-sought for goal since the appreciation of the relevance of the MRI to astrophysical disks. By necessity, a key piece of this puzzle consists of understanding the role that the various factors, both physical and numerical, play in the saturated state. In this *Letter*, we provide an expression that describes the transport of angular momentum in shearing MHD boxes, based on a series of local numerical simulations carried out by Sano et al. (2004). In particular, we are able to disentangle how the characteristics of the MHD flow depend on the various physical (pressure, magnetic field, etc.) and numerical (box size and resolution) factors.

## 2. CHARACTERISTIC SCALES IN NUMERICAL SIMULATIONS

Electronic address: mpessah@ias.edu (MEP)

<sup>1</sup> Institute for Advanced Study, Princeton, NJ, 08540<sup>2</sup> Institute for Theory and Computation, Harvard-Smithsonian Center for Astrophysics, Cambridge, MA, 02138<sup>3</sup> Astronomy Department, University of Arizona, Tucson, AZ, 85721<sup>4</sup> Physics Department, University of Arizona, Tucson, AZ, 85721

Numerical studies addressing the local dynamics of three-dimensional, differentially rotating, turbulent magnetized flows are often carried out in the shearing box approximation. This consists of a first order expansion in the variable  $r - r_0$  of all the quantities characterizing the flow at the fiducial radius  $r_0$ . The goal of this approach is to retain the most relevant physics governing the dynamics of the MHD fluid in a locally-Cartesian coordinate system co-orbiting and corotating with the background flow with local velocity  $v_0 = r_0 \Omega_0 \hat{\phi}$ .

In the shearing box framework, all the physical variables are usually normalized using the initial density,  $\rho_0$ , and the angular velocity,  $\Omega_0$ . For a more detailed discussion concerning the physical approximations and numerical implementations involved in the shearing box approach see Hawley et al. (1995). In an unstratified shearing box there are three possible scales of length relevant to the vertical direction: (i) The first scale is the size of the box  $L$ . (ii) The second scale is the wavelength corresponding to the most unstable MRI mode, i.e.,  $\lambda_{\text{MRI}} \equiv 2\pi\sqrt{16/15}\bar{v}_{Az}/\Omega_0$ , where  $\bar{v}_{Az}$  is the average Alfvén velocity associated with the vertical component of the magnetic field,  $v_{Az} \equiv B_z/(4\pi\rho_0)^{1/2}$ , and we have assumed a Keplerian shear profile (i.e.,  $q = 3/2$ ). (iii) The last scale is associated with the sound speed:  $H \equiv (2/\gamma)^{1/2}c_s/\Omega_0$ , where  $\gamma$  is the ratio of specific heats and  $c_s$  is the speed of sound. In a stratified disk,  $H$  is the pressure scale-height and, for simplicity, we will refer to it as such hereafter, even though the particular simulations we will be discussing are not stratified.

Most systematic studies carried out to characterize the turbulent state driven by the MRI consider non-radiative flows in which the internal energy grows in time due to magnetic dissipation. Furthermore, most of the initial efforts to characterize the saturated state of the MRI employed numerical schemes that evolved the internal energy, as opposed to the total energy. In these cases the reported values of  $\alpha$ , as well as the expressions for different predictor functions, were obtained considering the initial pressure  $P_0$ . In such simulations, however, gas pressure increases linearly with time and this effect must be considered in order to understand its effects on the stresses responsible for angular momentum transport.

Sano et al. (2004), carried out a series of numerical simulations in order to investigate the effects of the evolving pressure on the turbulent state. They employed an algorithm that solves the energy equation in terms of the total energy, which allowed them to keep better track of the energy budget of the flow. By considering the vertical extent of the box  $L$  as the unit of length, they were able to examine the dependence of the efficiency of angular momentum transport on the gas pressure. In this case, both the gas pressure  $P_0$  and the mean Alfvén velocity  $\bar{v}_{Az}$ , are independent parameters and determine the ratios  $H_0/L$  and  $\lambda_{\text{MRI}}/L$ , respectively, where the subscript zero indicates initial values.

### 3. SCALING LAWS IN MRI-DRIVEN TURBULENCE

Sano et al. (2004) performed an extensive set of simulations with zero net magnetic flux through the domain, initialized with a vertical magnetic field  $B_{0z}(r) = B_{0z} \sin[2\pi(r - r_0)/L_r]$ , and runs with a uniform magnetic field,  $B_{0z}$ , perpendicular to the disk midplane<sup>5</sup>. They investigated adiabatic

<sup>5</sup> Note that in both of these cases the magnetic flux through the domain is conserved because of the adopted vertical periodic boundary conditions.

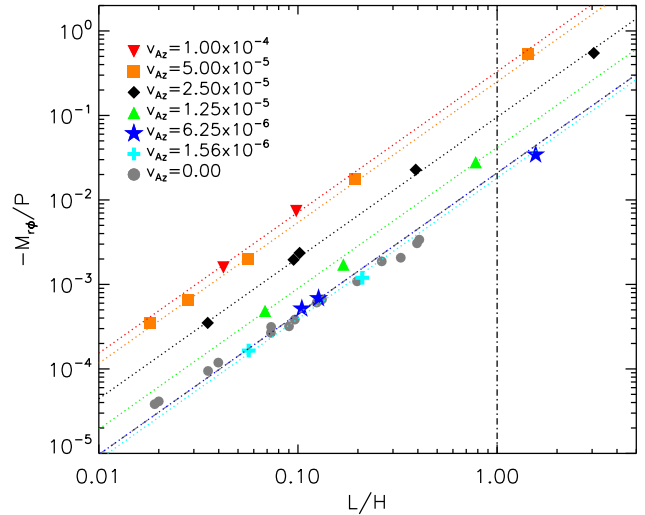


FIG. 1.— Dimensionless magnetic stress, normalized by the instantaneous pressure, as a function of a dimensionless measure of the box size with respect to the evolving scale-height,  $H = H_0(\bar{P}/P_0)^{1/2}$ , for the numerical simulations of Sano et al. (2004). The various types of symbols label simulations according to the value of the ratio  $\bar{v}_{Az}/L\Omega_0$ , with  $L = 1$  and  $\Omega_0 = 10^{-3}$ . The *dotted lines* are the best fits for each set of simulations with constant ratio  $\bar{v}_{Az}/L\Omega_0 \neq 0$ . The *dashed line* is the best fit for all the simulations with zero net magnetic flux. In all the cases a constant slope of  $5/3$ , i.e.,  $\bar{M}_{r\phi}/\bar{P} \propto (L/H)^{5/3}$ , provides a remarkably good description of the simulation results.

( $\gamma = 5/3$ ) as well as isothermal ( $\gamma = 1.001$ ) equations of state. They also performed a suite of runs to study the effects of Ohmic dissipation but we will not discuss them here. For all their models they used a shearing box with dimensions  $L = L_r = L_z = 1$  and  $L_\phi = 4L$ , and a grid of  $32 \times 128 \times 32$  zones. The scales of density and time are the same as in Hawley et al. (1995), i.e.,  $\rho_0 = 1$  and  $\Omega_0 = 10^{-3}$ .

Their choice of initial conditions spans six orders of magnitude in the initial pressure  $P_0$  and two orders of magnitude in the Alfvén speed. Figure 1 shows the dimensionless ratios  $\bar{M}_{r\phi}/\bar{P}$  as a function of the ratio  $L/H$  characterizing the turbulent states reached by the adiabatic and isothermal simulations listed in Tables 1 and 2 in Sano et al. (2004). Here,  $\bar{M}_{r\phi} \equiv \langle \langle \delta B_r \delta B_\phi \rangle \rangle / 4\pi$ ,  $\bar{P}$ , and  $H$  stand for the volume- and time- averaged values of the magnetic stress, pressure, and, equivalent scale-height  $H = H_0(\bar{P}/P_0)^{1/2}$ .

The tight correlations followed by simulations characterized by the same values of mean Alfvén velocities, including the class of simulations with zero net magnetic flux, i.e.,  $\bar{v}_{Az} = 0$ , suggest the scaling

$$\left. \frac{\bar{M}_{r\phi}}{\bar{P}} \right|_{\bar{v}_{Az}/L\Omega_0 = \text{const.}} \propto \left( \frac{L}{H} \right)^{5/3}. \quad (1)$$

The best fits to the data are shown in Figure 1 with a *dashed line* and *dotted lines* for simulations with zero and non-zero net magnetic flux, respectively. This scaling<sup>6</sup> can be used to remove the dependence of the ratio  $\bar{M}_{r\phi}/\bar{P}$  on  $L/H$  for each set of simulations with the same value of the ratio  $\bar{v}_{Az}/L\Omega_0$ . The result is shown in Figure 2, where the various types of symbols label the best fit values characterizing each class of simulations according to their value of  $\bar{v}_{Az}/L\Omega_0$ . The error

<sup>6</sup> Note that fixing all the slopes to  $5/3$  in Fig. 1 allows us to describe all the simulations on the same footing while leading to small residuals in the best fit amplitudes (see Fig. 2)

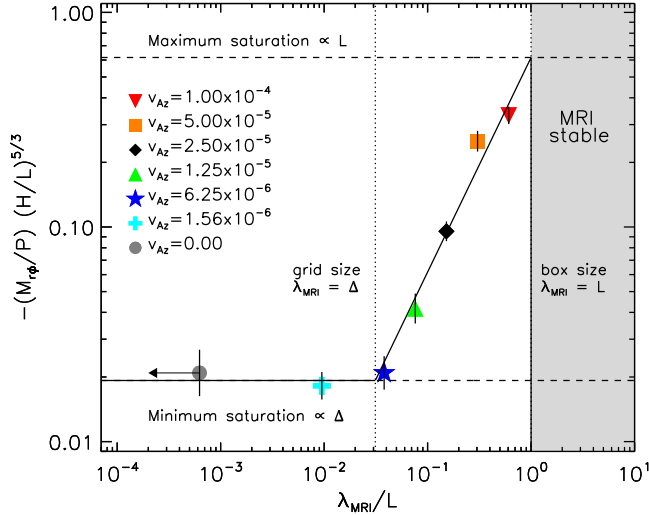


FIG. 2.— Dimensionless magnetic stress,  $-\bar{M}_{r\phi}/\bar{P}$ , multiplied by  $(H/L)^{5/3}$ , as a function of the wavelength corresponding to the most unstable MRI mode,  $\lambda_{\text{MRI}}$ . The various types of symbols correspond to the best fit values characterizing each class of simulations according to the value of the ratio  $\bar{v}_{Az}/L\Omega_0$ , as inferred from Figure 1. The simulations with zero mean magnetic flux, i.e.,  $\bar{v}_{Az} = 0$ , are displayed at some arbitrary value for visualization purposes only. The error bars quantify the scatter within each class of simulations around the corresponding mean values. Vertical dotted lines represent the values at which the most unstable MRI wavelength equals the grid size and the size of the box, respectively, i.e.,  $\lambda_{\text{MRI}} = \Delta = 1/32$  and  $\lambda_{\text{MRI}} = L = 1$ . The overall dependence of the saturation level on the ratio  $\lambda_{\text{MRI}}/L$  (solid line) is given by the saturation predictor (3). Numerical simulations for which  $\lambda_{\text{MRI}} > L$  are stable to the MRI (shaded region).

bars quantify the scatter within each class of simulations from the best fit values obtained in Figure 1. These average values follow a simple, yet tight, correlation with the associated values of  $\lambda_{\text{MRI}}$ .

The vertical dotted lines in Figure 2 represent the values at which the most unstable MRI wavelength equals the size of the box and the grid size, respectively, i.e.,  $\lambda_{\text{MRI}} = L = 1$  and  $\lambda_{\text{MRI}} = \Delta = 1/32$ . Note that numerical simulations for which  $\lambda_{\text{MRI}} > L$  are stable to the MRI (shaded region). The saturation of the simulations for which  $\Delta < \lambda_{\text{MRI}} \leq L$  is linearly proportional to  $\lambda_{\text{MRI}}$ , i.e.,

$$\frac{\bar{M}_{r\phi}}{\bar{P}} \left(\frac{H}{L}\right)^{5/3} \propto \lambda_{\text{MRI}}. \quad (2)$$

Note that Sano et al. (2004) concluded that  $\bar{M}_{r\phi} \propto \bar{v}_{Az}^{3/2} \propto \lambda_{\text{MRI}}^{3/2}$ . This steeper dependence does indeed provide a good description of the simulations with  $\bar{v}_{Az} = 5 \times 10^{-5}, 2.5 \times 10^{-5}, 1.25 \times 10^{-5}$ . However, a linear dependence on  $\bar{v}_{Az}$  leads to a better overall description of all the simulations with  $\Delta < \lambda_{\text{MRI}} \leq L$ , i.e., including those with  $\bar{v}_{Az} = 6.25 \times 10^{-6}$  and  $\bar{v}_{Az} = 1 \times 10^{-4}$ .

There is a clear departure from the linear dependence of the saturated stress on  $\bar{v}_{Az}$  for the simulations for which  $\lambda_{\text{MRI}} \leq \Delta$ . All of these runs saturate at the same value of  $(\bar{M}_{r\phi}/\bar{P})(H/L)^{5/3}$  regardless of the value of the magnetic flux through the vertical boundary. The fact that this minimum value of the stresses at saturation (lower dashed line in Figure 2) is equal to 1/32 of the maximum possible value, corresponding to  $\lambda_{\text{MRI}} = L$  (upper dashed line in the same Figure), strongly suggests that this floor is entirely set by the grid size. Extrapolating this behavior to lower values of the grid scale suggests that this minimum saturation level is itself

linearly proportional to the size of the grid<sup>7</sup>. This is consistent with the results found in Hawley et al. (1996); see in particular their Figure 8, where the final plasma  $\beta$ 's for simulations with zero net magnetic flux and uniform vertical magnetic fields is shown. The ratio of the final plasma  $\beta$  for the simulation with highest uniform field to the average final plasma  $\beta$  corresponding to the zero net magnetic flux runs is indeed close to  $\Delta = 1/32$ .

The overall dependence of the saturation level on the ratio  $\lambda_{\text{MRI}}/L$ , i.e., the solid line in Figure 2, is described by the function

$$\frac{\bar{M}_{r\phi}}{\bar{P}} \simeq -0.61 \left(\frac{L}{H}\right)^{5/3} \times \begin{cases} \Delta/L & \text{if } \lambda_{\text{MRI}} \leq \Delta \\ \lambda_{\text{MRI}}/L & \text{if } \Delta < \lambda_{\text{MRI}} \leq L \\ 0 & \text{if } \lambda_{\text{MRI}} > L \end{cases}. \quad (3)$$

This saturation predictor is consistent, in the intermediate regime, with the one obtained by Hawley et al. (1995) that we also used in an earlier work (Pessah et al. 2006b). Indeed, substituting in this expression  $\bar{P} = P_0 = \rho_0(H_0\Omega_0)^2$ ,  $H = H_0 = L$ , and considering that the magnetic stress is roughly half of the magnetic energy in the fluctuations,  $\bar{M} \equiv \langle \delta B^2 \rangle / 8\pi$  (Blackman, Penna, & Varniere 2006, and references therein), leads to

$$\bar{M} = 1.2\rho_0(L\Omega_0)(\lambda_{\text{MRI}}\Omega_0), \quad (4)$$

which is identical to equation (18) of Hawley et al. (1995).

The 5/3 scaling in the saturation predictor (3) is reminiscent of the Kolmogorov spectrum of turbulence. The prominent role of  $\lambda_{\text{MRI}}$  in this expression is another indication that the MRI continues to pump the turbulence, even in the non-linear state (see also Pessah et al. 2006a, 2006b). The dependence of the stress on the vertical size of the box,  $L$ , must be an artifact of the periodic boundary conditions, which do not allow for any turbulent energy to escape the domain of solution. The dependence on the resolution must be related to numerical dissipation at the grid scale, and might, therefore, change if a different MHD algorithm were used for the simulations. Finally, the role of the “scale-height”,  $H$ , is very difficult to understand, since the simulations are not stratified and this length scale is too large to be resolved. It may arise from a non-linear coupling between sound waves and MHD modes or it might simply be related to numerical dissipation through the dependence of the Courant time step on sound speed.

#### 4. IMPLICATIONS AND DISCUSSION

In shearing-box simulations of Keplerian flows, the Maxwell and Reynolds,  $\bar{R}_{r\phi} \equiv \langle \rho \delta v_r \delta v_\phi \rangle$ , stresses follow a tight correlation (see Pessah, Chan, & Psaltis 2006a, and references therein) with  $-\bar{M}_{r\phi}/\bar{R}_{r\phi} \simeq 4$ . Taking this into account, we can write for the total stress and the effective alpha viscosity

$$\frac{\bar{T}_{r\phi}}{\bar{P}} = q\alpha \simeq 0.75 \left(\frac{L}{H}\right)^{5/3} \times \begin{cases} \Delta/L & \text{if } \lambda_{\text{MRI}} \leq \Delta \\ \lambda_{\text{MRI}}/L & \text{if } \Delta < \lambda_{\text{MRI}} \leq L \\ 0 & \text{if } \lambda_{\text{MRI}} > L \end{cases}, \quad (5)$$

<sup>7</sup> After this paper appeared on the preprint server, Fromang and Papaloizou posted a paper (arXiv:0705.3621) in which they perform ideal MHD simulations for zero-net-field shearing boxes with increasing resolution. They found that the saturated stresses depend linearly on resolution, in agreement with the results presented here.

where  $q = 3/2$  for a Keplerian disk. This is a remarkable result. This expression accurately describes the overall dependence of the saturated state for 35 numerical simulations spanning six orders of magnitude in initial pressure, encompassing domains with zero and non-zero net magnetic flux, as well as adiabatic and isothermal equations of state.

Note that the very small values of the effective alpha viscosity reported in the past, which are unable to account for observations of astrophysical disks (King, Pringle, & Livio 2007), correspond to shearing box simulations with vertical extents that are small compared to the equivalent pressure scale-height. One would expect that a realistic value of the stress is achieved in simulations with  $L \simeq H$ . Nevertheless, even having taken this into account, large values of the alpha viscosity can be achieved only for particular configurations. This has three important implications for accretion disk models in which the angular momentum transport is mediated by MRI-driven turbulence.

First, the saturated stresses in simulations with zero net magnetic flux are linearly proportional to the numerical resolution. This implies that if we were able to set the numerical resolution to the natural dissipation scale in the problem, which is many orders of magnitude smaller than the pressure scale height, the MRI would be unable to sustain the necessary turbulent stresses in a Keplerian shearing box, unless there were a significant magnetic flux through the vertical box boundaries.

Second, in order for MRI-driven turbulence to account for the large values of the effective alpha viscosity inferred from observations ( $\alpha \gtrsim 0.1$ ; see King et al. 2007), the vertical magnetic field must grow to a strength such that the most unstable MRI-modes have wavelengths comparable to the disk scale-height, i.e.,  $\lambda_{\text{MRI}} \simeq L \simeq H$ . Such vertical fields are only a small fraction, roughly a few hundredths, of the associated equipartition field and pose no significant problem to the energy budget of the accretion flow. Indeed, the origin of such a small mean magnetic field perpendicular to

the disk midplane need not be external to the disk. MRI-driven fluctuations can easily give rise to magnetic fields of this order, perhaps through the combined effects of shearing, MRI, and Parker instability, as in the mechanism proposed by Tout & Pringle (1992). Note that disk stratification is likely to play an important role in driving helical turbulence and thus in enabling the development of a global, large-scale magnetic flux (Brandenburg, Nordlund, Stein, & Torkelsson 1995; Tan & Blackman 2004; Blackman & Tan 2004).

Finally, in MRI-driven turbulence, the turbulent magnetic energy is comparable to  $\bar{T}_{r\phi}$  (Pessah, Chan, & Psaltis 2006a) and, hence, will have to be also comparable to the thermal energy, if  $\alpha$  is of order unity. This implies that the vertical scale height of an accretion disk is set by both the magnetic and the thermal pressures, with important implication for the spectrum emerging from each disk annulus (Blaes et al. 2006) as well as for the viscous and thermal stability of the disk.

In closing, it is important to remark that the saturation predictor (5) may be specific to shearing-box simulations with periodic boundary conditions and not necessarily applicable to the local saturation of stresses in stratified (e.g., Brandenburg, Nordlund, Stein, & Torkelsson 1995; Miller & Stone 2000) or global simulations (e.g., Armitage 1998; Hawley 2000, 2001). In these cases, the physical mechanism that limits the growth of turbulent magnetic energy maybe related to magnetic buoyancy or to large meridional circulation. In both mechanisms, magnetic energy is lost at large scales and, therefore, the dependence of the saturated stress on the numerical resolution and the sound speed may disappear. Understanding the physical origin of the saturation predictor (5) and comparing it to simulations of stratified shearing boxes will resolve these issues.

We thank Eric Blackman, Jeremy Goodman, Gordon Ogilvie, and Jim Stone for valuable comments and discussions.

#### REFERENCES

- Armitage, P. J. 1998, *ApJ*, 501, L189  
 Balbus, S. A. & Hawley J. F. 1991, *ApJ*, 376, 214  
 ———. 1998, *Rev. Mod. Phys.*, 70, 1  
 Balbus, S. A. & Papaloizou J. C. B. 1999, *ApJ*, 521, 650  
 Blackman, E. G., Penna, R. F., & Varniere, P. 2006, [astro-ph/0607119]  
 Blackman, E. G. & Tan, J. C. 2004, *Ap&SS*, 292, 395  
 Blaes, O. M., Davis, S. W., Hirose, S., Krolik, J. H., & Stone, J. M. 2006, *ApJ*, 645, 1402  
 Brandenburg, A., Nordlund, A., Stein, R. F., & Torkelsson, U. 1995, *ApJ*, 446, 741  
 Brandenburg, A. 1998, in *Theory of Black Hole Accretion Discs*, Abramowicz, M. A., Björnsson, G., & Pringle, J. E., eds., Cambridge University Press (Cambridge)  
 Frank, J., King A., & Raine, D. J. 2002, *Accretion Power in Astrophysics*, 3rd edn., Cambridge University Press (Cambridge)  
 Fromang, S. & Papaloizou, J. 2007, [arXiv:0705.3621]  
 Gammie C.F. 1998, in *Accretion Processes in Astrophysical Systems: Some Like it Hot!*, S.S., Holt, T.R. Kallman, AIPC 431, 99  
 Hawley, J. F. 2000, *ApJ*, 528, 462  
 ———. 2001, *ApJ*, 554, 534  
 Hawley, J. F., Gammie, C. F., & Balbus, S. A. 1995, *ApJ*, 440, 742  
 ———. 1996, *ApJ*, 464, 690  
 Kato, S., Fukue, J., & Mineshige, S. 1998, *Black-Hole Accretion Discs*. Kyoto University Press (Kyoto)  
 Kato, S. & Yoshizawa, A. 1995, *Publ. Astron. Soc. Jap.*, 47, 629  
 King, A. R., Pringle, J. E., & Livio, M. 2007, *MNRAS*, 376, 1740  
 Miller, K. A. & Stone, J. M. 2000, *ApJ*, 534, 398  
 Ogilvie, G. I. 2003, *MNRAS*, 340, 969  
 Pessah, M. E., Chan C. K., & Psaltis, D. 2006a, *MNRAS*, 372, 183  
 ———. 2006b, *Phys. Rev. Lett.*, 97, 221103  
 ———. 2007, *MNRAS*, submitted, [astro-ph/0612404]  
 Sano, T., Inutsuka, S. I., & Miyama, S. M. 1998, *ApJ*, 506, L57  
 Sano, T., Inutsuka, S. I., Turner, N. J., & Stone, J. M. 2004, *ApJ*, 605, 321  
 Shakura, N. I. & Sunyaev, R. A. 1973, *A&A*, 24, 337  
 Tan, J. C. & Blackman, E. G. 2004, *ApJ*, 603, 401  
 Tout, C. A. & Pringle, J. E. 1992, *MNRAS*, 259, 604